Journal of Alloys and Compounds 509 (2011) 6311–6316

Contents lists available at ScienceDirect

Journal of Alloys and Compounds

journal homepage: www.elsevier.com/locate/jallcom

Electrical, magnetic, and magnetoelectric characterization of fine-grained $Pb(Zr_{0.53}Ti_{0.47})O_3$–$(Ni_{0.5}Zn_{0.5})Fe_2O_4$ composite ceramics

Hong-fang Zhang[a], Siu Wing Or[a,*], Helen Lai Wa Chan[b]

[a] Department of Electrical Engineering, The Hong Kong Polytechnic University, Hung Hom, Kowloon, Hong Kong
[b] Department of Applied Physics, The Hong Kong Polytechnic University, Hung Hom, Kowloon, Hong Kong

ARTICLE INFO

Article history:
Received 25 November 2010
Received in revised form 9 March 2011
Accepted 13 March 2011
Available online 21 March 2011

Keywords:
Magnetoelectric composite ceramics
Piezoelectric ceramics
Magnetosrictive materials
Ferrite
Fine grain

ABSTRACT

Fine-grained $Pb(Zr_{0.53}Ti_{0.47})O_3$–$(Ni_{0.5}Zn_{0.5})Fe_2O_4$ (PZT–NZFO) magnetoelectric (ME) composite ceramics were fabricated by a modified hybrid process at a low sintering temperature of 900 °C. Well-controlled crystallized grain size and homogeneous microstructure with a good mixture of two phases were observed in the ceramics. The ceramics show coexistence of ferrimagnetic and ferroelectric phases with well-formed ferromagnetic and ferroelectric hysteresis loops at room temperature. A significant ME effect was observed with a ME coefficient of 0.537 V cm^{-1} Oe^{-1} in the vicinity of electromechanical resonance. In addition, high capacitance can be obtained at low frequency, and magnetic properties in the ceramics can be tailored by the grain size of the ferromagnetic particles in a simple and flexible way.

1. Introduction

The magnetoelectric (ME) effect in ferrite-piezoelectric composite ceramics is a "product property", since the ME coefficient $\alpha_E = \delta E/\delta H$ is the product of the magnetostrictive deformation $\delta z/\delta H$ and the piezoelectric field generation $\delta E/\delta z$ [1]. Due to their attractive physical properties and potential applications in actuators, transducers, magnetic field sensors and data storage devices, there has been continued interest in the study of ME materials in the past decades [2–4]. Although remarkable progress in ME materials has been made by using bilayers and multilayers [5–12], which are reported to possess ME coefficient of 3–230 times that in single-phase materials, such as Cr_2O_3 (showing such a weak ME effect that they have not yet found any technological applications) [13]. However, it is difficult to overcome the drawbacks which include high eddy-current losses at high frequencies, mechanical brittleness, and weak mechanical modulus of the constituents using polymer binder. Bulk composites ceramics are desirable over layered samples due to superior mechanical strength. One could also easily control the physical, magnetic, electrical and ME parameters with proper choice in the two phases and their volume fractions [14–20]. Unfortunately, the theoretical coefficient is larger than the experimental one (e.g. theory: 2400 mV^{-1} cm^{-1} Oe^{-1}) [21], which is mainly due to some defects. Undesired phases and interphase diffusion of the constitutional atoms, caused by interdiffusion and/or chemical reactions between the ferrite and piezoelectric phases during conventional high-temperature sintering have led to the change in the properties of the ferrite and piezoelectric phases, giving rise to high leakage currents. Moreover, due to the leakage current problem, the electric poling of the ceramics becomes difficult and the strength of the ME interactions is reduced. In addition, the thermal expansion mismatch would result in pores and the formation of microcracks in the ceramics, owing to the different sintering behaviors of the constituent ferrite and piezoelectric phases under a condition of high temperature sintering beyond 1000 °C. Probably because the components are not fully in contact, transfer of elastic strasses with losses would deteriorate the ME response of the ceramics. Thus, a necessary condition for ME ceramic is a perfect coupling between the phases. Nowadays, most studies on such ceramics consisting of ferrite and piezoelectric phases have mainly focused on how to maximize their ME coefficients. In this experiment, well-developed and fine-grained PZT–NZFO ME composite ceramics with dense, homogeneous microstructures are produced by a modified hybrid process at a low sintering temperature of 900 °C for 4 h. The finer microstructure obtained at low sintering temperature is expected to give sufficient bulk density and high mechanical strength while avoiding defects occurring between the two phases, besides mitigating the element evaporation and inhibiting the formation of pores and microcracks in the ceramics. A glassy component coated nano-sized piezoelectric PZT powders as a liquid phase in the matrix is employed to modify the interfacial contact of the individual particles as well as to enhance the

* Corresponding author. Tel.: +852 3400 3345; fax: +852 2330 1544.
E-mail address: eeswon@polju.edu.hk (S.W. Or).

0925-8388/$ – see front matter © 2011 Elsevier B.V. All rights reserved.
doi:10.1016/j.jallcom.2011.03.071

crystallization of PZT phase during the low temperature sintering course. As a result, an enhanced ME interaction in the fine-grained PZT–NZFO ceramics can be achieved. Detailed discussion on the sintering behavior, microstructures, magnetic and electrical properties of the ceramics along with their ME effects are reported.

2. Experimental

2.1. Formation of fine-grained PZT–NZFO composite ceramics

2.1.1. Nano-sized crystalline PZT powders coated by a glassy phase prepared by a modified hybrid processing

Firstly, a modified hybrid processing was employed to prepare nano-sized crystalline PZT particulates coated by the dried $PbO–B_2O_3–SiO_2$ (PBS) glass gel powders. The process route included: $PbO–B_2O_3–SiO_2$ (PBS) ternary phase with the molar ratio of 40:40:20 was selected and used in the crystallization of $Pb(Zr,Ti)O_3$. The concentration of the PBS glass solution was adjusted to 1 M, 100 ml with the solvent ethanol. The dried PBS gel powder was obtained after heating at 120 °C for 10 h. Nano-sized crystalline PZT powders was prepared using a polymer modified sol–gel method [15] and calcined at 800 °C for 2 h. Crystaline size of the PZT particles was found to be ~16 nm [Calculated from the XRD pattern (not shown) using the Scherrer's equation] [22]. The PZT powders were dispersed into the PBS dried gel solution (dis9solved in ethanol instead of the PBS sol precursor solution), and mixed thoroughly to form PZT–PBS powder slurry by conventional ball milling for 2 h. The mass ratio of the PBS gel powders to the nano-sized PZT particles was 5 wt% to give a balance between the processing behavior and properties of the resulting ceramics. Finally, the as-prepared uniformly distributed PZT–PBS slurry was dried at 120 °C, calcined at 450 °C for 2 h, and was ready for further processing.

2.1.2. Preparation of fine-grained PZT–NZFO composite ceramics

Firstly, the submicron-sized crystalline NZFO powders with an average size of ~100–500 nm were calcined at 1000 °C for 2 h by a conventional solid state sintering (as described in previous report [15]). Then, the calcined nano-sized PZT powder coated by glassy phase was mixed with the NZFO powder by ball milling for 2 h and the resulting ceramic slurry was dried at 150 °C for 10 h. The granulated powders were uniaxially pressed into disk samples (13 mm diameter, 0.5–0.7 mm thickness) at a pressure of 4 MPa in a stainless steel die. All the specimens were sintered in air at 900 °C for 4 h. In the present work, wt% ratios of NZFO powders and glass-coated nano-sized PZT powders of 10/90, 15/85, 25/75, 50/50 and 60/40 were fabricated (denoted as 10 wt%, 15 wt%, 25 wt%, 50 wt% and 60 wt% ceramics).

2.2. Property measurements

The phase structure and morphology of the ceramics were observed by X-ray diffraction (XRD, Philips X'Pert-Pro MPD) with CuKα1 radiation (1.5406 Å, 40 kV, 30 mA) at room temperature and field emission scanning microscopy (SEM, JEOL JSM-6335F), respectively. The elemental analysis was done by energy dispersive X-ray spectroscopy (EDX) during the SEM measurements. Magnetization measurements were performed on a vibrating sample magnetometer (VSM, Lakeshore 7300 series, USA) at room temperature.

To study the electrical and piezoelectric properties, low temperature fired-on silver paste was applied onto both sides of the ceramics and heat-treated at 600 °C for 30 min to form silver electrodes. The dielectric spectrum was measured with an Agilent 4294A impedance analyzer. The temperature dependence of relative permittivity at various frequencies was investigated at a heating rate of 2 °C/min using a computer-controlled automated system consisted of the impedance analyzer, a temperature-controlled furnace (Carbolic), and a multimeter (Keithley 2000) as the temperature controller. The polarization–electric field (P–E) hysteresis loop measurement for the composites was carried out using a modified Sawyer Tower circuit at a frequency of 1 kHz at room temperature. The piezoelectric constant d_{33} was measured by a standard piezo d_{33} meter. The ME coefficient (α_E) of the ceramics was characterized using an in-house automated measurement system.

3. Results and discussion

3.1. Characteristics of sintering behavior and microstructures

Fig. 1 shows the X-ray diffraction (XRD) patterns of PZT–NZFO ceramics at various mixing ratios. In Fig. 1(a), the diffraction pattern of NZFO powders calcined at 1000 °C is characterized as a pure, crystalline NZFO with a spinel structure. For nano-sized PZT powders coated by glass calcined at 450 °C [Fig. 1(b)], all the peaks exhibit the presence of pure PZT with a perovskite structure. The results indicate the success in synthesizing low temperature sintering nano-sized PZT powders coated by glass using the modified hybrid processing route. As for the sintered ceramics with 10, 15, 25, 50 and 60 wt% of NZFO contents [Fig. 1(c)–(g)], the peaks consist of peaks from both ferroelectric (PZT phase) and ferrimagnetic (NZFO phase) components. All the peaks can be identified and no intermediate phase is observed by using XRD, which indicate there is no third phase in the sintered ceramics.

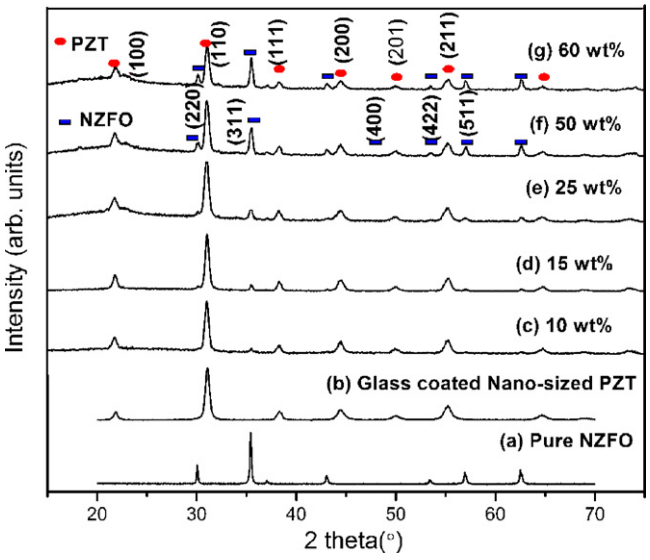

Fig. 1. XRD patterns of the PZT–NZFO ceramics with various amounts of NZFO contents sintered at 900 °C for 4 h, together with pure NZFO and glass-coated nano-sized PZT powders, respectively: (a) pure NZFO powders calcined at 1000 °C, (b) glass-coated nano-sized PZT powders at 450 °C, and ceramics with (c) 10 wt%, (d) 15 wt%, (e) 25 wt%, (f) 50 wt%, and (g) 60 wt% NZFO.

Fig. 2 shows the natural top surface morphologies of the ceramics with different NZFO contents: (a) 15 wt%, (b) 25 wt%, and (c) 50 wt%. As shown in Fig. 2, dense, homogeneous, and well-developed fine grains are obtained at low firing temperature. The EDX results suggest that grains of average size of 1–2 μm are the PZT and that of sizes below 500 nm are the NZFO phase which are both found in the ceramics. One can clearly see that the grain sizes of the NZFO phase (about 100–500 nm) remain unchanged in all the well-sintered samples. Since well crystallized NZFO powders are used as template (i.e. 3–0 connectivity pattern) for the in-situ preparation of the powder ceramics, the subsequent sintering for promoting the PZT grain growth practically does not change the crystallization of the NZFO component. Besides, the grain sizes of PZT phase in the ceramics are well-controlled and are quite uniform with no large grains observed, which denotes that excessive grain growth could be overcome by the modified hybrid process. For various compositions of PZT–NZFO ceramics sintered at the same temperature, the proportion of the two phases determined from the relative peak intensity ratios of the parented phases roughly agrees with the nominal values [Fig. 1(c)–(g)].

The hybrid process has been reported by us in previous reports [23,24]. The main feature is to combine the merits of high crystallinity and high performance of nanocrystalline powders with those of low sintering temperature such as the sol–gel wet chemistry process, and it is easy to achieve a modification of the processing behaviors of ceramics, which is useful to produce fine-grained and high-performance ceramics at low sintering temperatures. In addition, the well-dispersed glass component by the modified hybrid process used in this work also plays the role of a liquid in the matrix, reducing the interpowders friction, aiding rapid rearrangement of the solid powders, which results in more efficient packing between powders from individual phase giving rise to a very good mixing in the ceramic body.

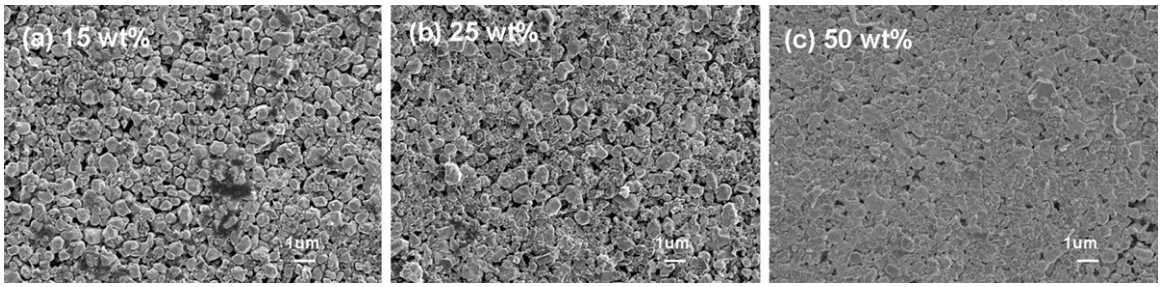

Fig. 2. SEM micrographs of the surface of ceramics with various amounts of NZFO contents: (a) 15 wt%, (b) 25 wt%, and (c) 50 wt%.

3.2. Magnetic properties

Figs. 3(a) and (b) show the room-temperature magnetic hysteresis loops of PZT–NZFO ceramics with various NZFO contents, together with the saturation magnetization (M_s) and coercive field (H_c), respectively. In Fig. 3(a), the ceramics exhibit typical magnetic hysteresis loops, indicating the presence of an ordered magnetic structure. Both the saturation (M_s) and remanent (M_r) magnetizations [in the inset of Fig. 3(a)] increase with increasing wt% of NZFO content in the ceramics. This means that magnetization can be realized in the presence of nonmagnetic PZT. For instance, for the ceramic with 15 wt% NZFO content, M_s and M_r are found to be 13.462 emu/g and 0.922 emu/g, respectively, while for the ceramic with 60 wt% NZFO content, the M_s and M_r are 53.355 emu/g and 6.626 emu/g, respectively. In Fig. 3(b), it is interesting to find that the low coercive field (H_c) of ~32–33 Oe is obtained and it remains nearly constant in the ceramics. The coercive field shows a slight change and may be explained as follows. According to an improved Stoner–Wohlfarth model, the phenomenological relation for a spherical finer particle [25] can be given by Eq. (1):

$$K_{eff} = K_b + \frac{6}{d}K_s \quad (1)$$

where K_{eff} is the overall anisotropy constant per unit volume of the powder, K_b the bulk uniaxial anisotropy constant per unit volume, K_s the surface anisotropy constant per unit area, and d is the diameter of the powder. Because the coercive field is proportionally related to the anisotropy coefficient (i.e. $H_c \propto K_{eff}$). As mentioned above, K_{eff} mainly depends on the diameter of the well-crystallized NZFO powders used as template in the ceramics. Therefore, K_{eff} can be approximately regarded as a constant. That is, all the magnetic properties can be well-preserved, which is one feature of the ceramics presented in this work. It shows that we can design the magnetic parameters (such as permeability, magnetostriction, and coercive field) of the ceramics by tailoring the grain sizes of the starting NZFO phase powders in an easy, flexible, and reproducible way.

3.3. Electrical properties

3.3.1. Dielectric properties

The room-temperature variations of dielectric constant and loss tangent with frequency are shown in Figs. 4(a) and (b) for the ceramics with NZFO contents of 10 – 60 wt%, respectively. In Fig. 4(a), all the ceramics reveal with dielectric dispersion, large values of dielectric constant at lower frequencies (1 kHz) and then constant values at higher frequencies [100 kHz to 10 MHz, as shown in the inset of Fig. 4(a)]. For example, at 1 kHz, in the 10 wt% ceramic, the dielectric constant is about 8000, and the 15 wt% ceramic has a dielectric constant of 722. In the inset of Fig. 4(a), with increasing NZFO content, the dielectric constant decreases in the higher frequency range of 100 kHz to 10 MHz. The fall in dielectric constant at higher frequencies is attributed to the fact that the ferroelectric regions (PZT) are surrounded by nonferroelectric region. For instance, at 100 kHz, in the 10 wt% ceramic, the dielectric constant is about 566, and the 50 wt% ceramic has a dielectric constant of about 120.

The high dielectric constants measured at low frequencies might be attributed to the interfaces between the ferroelectric and ferrimagnetic phases which have significantly different conductivities. These interfaces cause an additional polarization, the interfacial polarization, which boosts the dielectric constant and is in agreement with Koop's phenomenological theory [26].

The variation of loss tangent with frequency is shown in Fig. 4(b). Similarly, at lower frequencies, the loss tangent is large and it decreases with increasing frequency. For instance, in the 10 wt% ceramic, loss tangent is 2.29 at 1 kHz, and 0.3 at 100 kHz, respectively; while in the 15 wt% ceramic, loss tangent is 0.6 at 1 kHz, and 0.09 at 100 kHz, respectively. Loss tangent is proportional to the 'loss' of energy from the applied field in the ceramics (in fact this

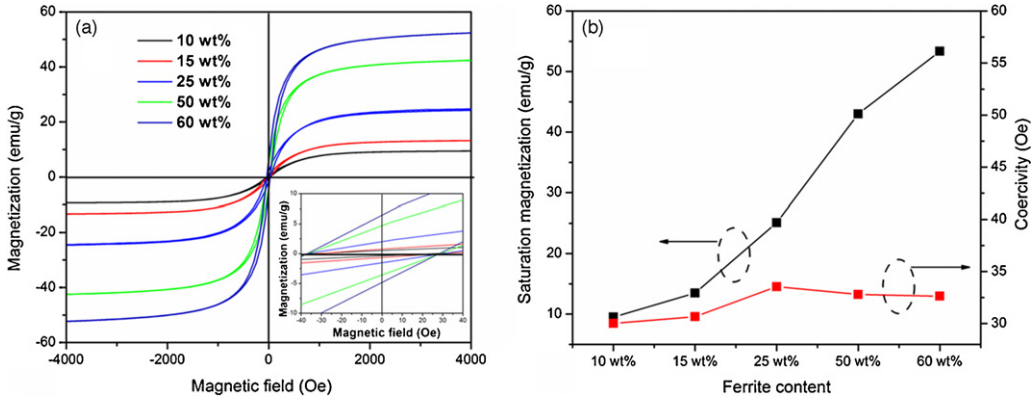

Fig. 3. (a) Magnetic hysteresis loops at room temperature of PZT–NZFO ceramics with different NZFO contents. The inset shows the low-field range of the loops. (b) The saturation magnetization (M_s), and coercivity (H_c) as a function of NZFO content of the ceramics.

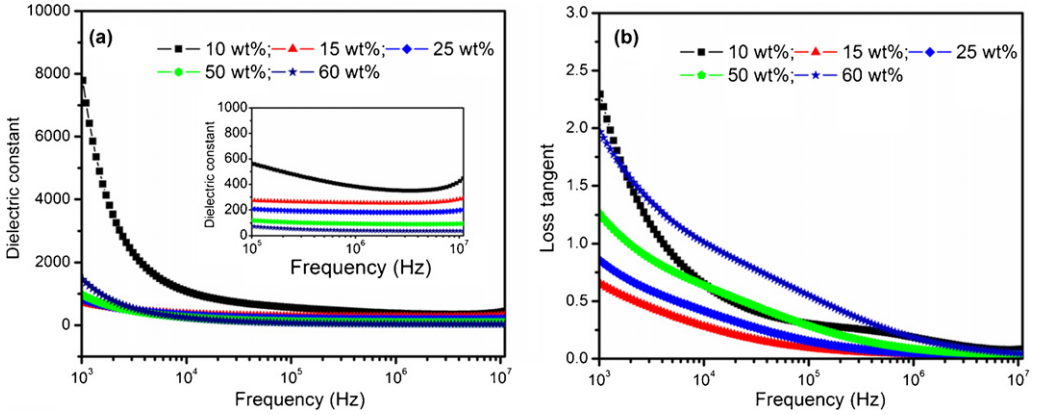

Fig. 4. Frequency dependence of (a) dielectric constant and (b) loss tangent of the ceramics. The insets in (a) shows the high-frequency range between 100 kHz and 10 MHz.

energy is dissipated into heat) and therefore denoted as dielectric loss. At low frequency, space charge polarization and electric conductivity contribute to the dielectric loss. At higher frequencies, the losses are reduced and the dipoles contribute to the polarization.

Figs. 5(a) and (b) show the variation in the dielectric constant and loss tangent as a function of temperature measured at different frequencies for the typical ceramic with NZFO content of 15 wt%, respectively. From the plots, it is seen that the dielectric constant of PZT–NZFO ceramic peaks at different temperatures and frequencies. Higher dielectric constants are obtained at lower frequencies, compared with pure PZT ceramics, the PZT–NZFO ceramics display a larger frequency dependence, exhibiting a mixture of normal ferroelectric behavior and relaxor characteristics. As described above, the interfacial polarization usually responds slowly to the external field, it is inactive at high frequencies (about 100 kHz to 1 MHz). Thus, it has no contribution to the dielectric constant at high frequencies, resulting in the decline of the dielectric constants. Moreover, the dielectric constant curves of our sample display a broad temperature dependence in the vicinity of the transition temperature (about 390 °C). This indicates that the sample has a strong tendency of diffused phase transition due to the finer microstructure. In addition, in Fig. 5(a), the dielectric constant of the sample at T_c does not obviously drop with increasing temperature at 1 kHz due to high conductivity in this temperature range. At high frequency of 100 kHz to 1 MHz, the decrease in dielectric constant is more evident than at lower frequency. The apparent increase in dielectric constant at elevated temperature is due to the increase conduction loss in this temperature range. This trend is consistent with the fact that PZT crystals surrounded by a glassy matrix have a higher electrical conductivity at higher temperature.

The variation of loss tangent with temperature is shown in Fig. 5(b). The plots are similar to the behavior of dielectric constant against temperature. At low frequencies, loss tangent is large and it decreases with increasing frequency. There is a rapid increase of loss tangent above 300 °C due to the high conductivity at high temperature.

3.4. Ferroelectric properties

Fig. 6 shows the polarization–electric field (P–E) hysteresis loop of the ceramic containing 15 wt% of NZFO content at the frequency of 1 kHz and room temperature. In Fig. 6, it is obvious that an apparent P–E loop is observed indicating that the ceramic is ferroelectric in character. The remanent polarization (P_r) is 0.75 μC/cm^2, and the coercive field (E_c) is 1.91 kV/mm. The ceramic is highly resistive with no breakdown under an applied electric field up to 5 kV/mm. Also, it is seen in Fig. 6 that the polarization hysteresis loop has a slightly shift to the right, which is presumably attributed to the space charge at low frequency.

3.5. Piezoelectric behavior

All the ceramics were poled perpendicular to the disk plane (z-axis) in silicone oil under a poling field of 2∼4 kV/mm and at temperature around 200 °C for 30 min. The piezoelectric characteristics were measured 24 h after poling. The piezoelectric characteristics of the ceramics containing 10, 15, 25, 50 and 60 wt% of NZFO content are investigated and shown in Fig. 7. As shown in Fig. 7, d_{33} (piezoelectric charge coefficient) decreases with the amount of the ferrite phase except for the 15 wt% ceramic. Also, g_{33} (piezoelectric

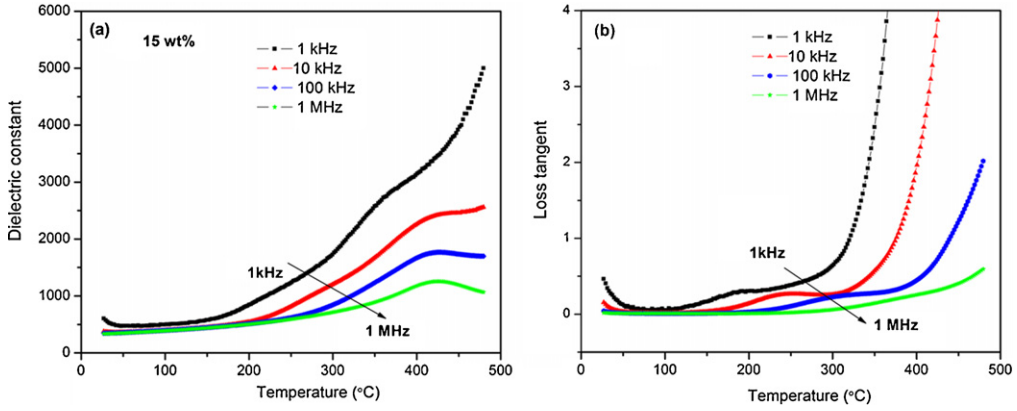

Fig. 5. Temperature dependence of (a) dielectric constant and (b) loss tangent of the 15 wt% ceramic, measured at the frequency range of 1 kHz to 1 MHz.

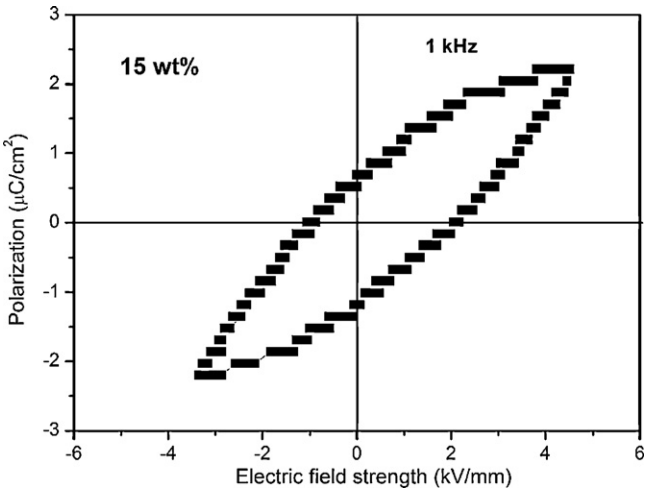

Fig. 6. Polarization-field hysteresis loop of the 15 wt% ceramic at the frequency of 1 kHz and room temperature.

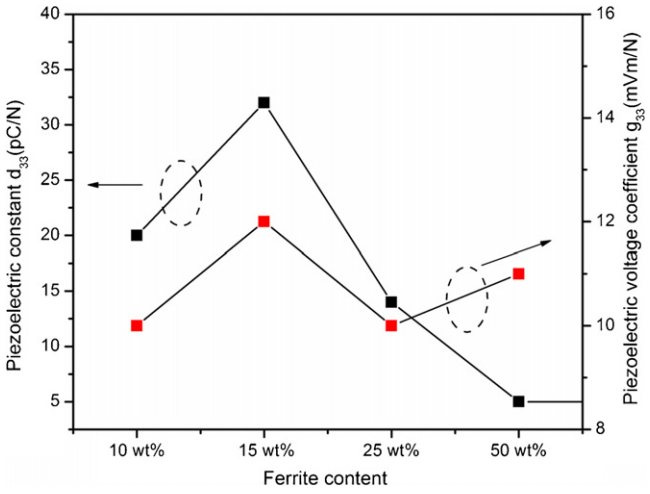

Fig. 7. Piezoelectric characteristics of the ceramics as a function of wt% of NZFO content.

voltage coefficient) changes slightly in the various compositions. In Fig. 7, the best piezoelectric property is obtained in the 15 wt% ceramic with d_{33} ~32 pC/N and g_{33} ~12 mVm/N.

3.6. ME voltage coefficient

ME characterization in the 15 wt% ceramic was studied by measuring the voltage response of the ceramic exposed to alternating and constant (bias) magnetic fields. The bias magnetic (H_{dc}) field was obtained using an electromagnet, and the alternating magnetic (H_{ac}) field was generated by a pair of Helmholtz coils. ME voltage coefficient was determined using $\alpha_E = \delta E/\delta H = \delta V/t{\cdot}\delta H$, where t is the effective thickness of the PZT phase (in this work, it was taken as 79% of the thickness of the ceramic since the densities of NZFO and PZT are 5.3 and 7.6 g/cm^3, respectively).The measurements were performed for the electric polarization vector parallel to the constant and alternating magnetic fields. Fig. 8(a) shows the frequency dependence of α_E, measured under a bias magnetic field (H_{dc}) up to 1 kOe and a superimposed alternating magnetic field (H_{ac}) of about 1 Oe amplitude with frequency varying from 1 to 200 kHz; and (b) shows α_E measured as a function of H_{dc} under a H_{ac} of 10 Oe at 1 kHz. In Fig. 8(a), it is noticed that α_E remains nearly constant in the low-frequency range of 1Hz to 150 kHz. A maximum α_E of 0.537 V cm^{-1} Oe^{-1} is observed under H_{ac} = 1 Oe at 166 kHz and H_{dc} = 1 kOe, which exhibits a resonance. We attribute the resonance in α_E to an electromechanical resonance in PZT. Electromechanical resonance (EMR) in ceramics consisting of the PZT phase was investigated through measurements of impedance Z or dielectric constant as a function of frequency (f). The inset of Fig. 8(a) shows such data for a poled 12.27 mm-diameter sample (used as α_E response). The impedance spectrum is found to exhibit a resonance peak at the same position as that observed in the ME measurements as a function of frequency. This further indicates that the peak was correlated with the electromechanical resonance mode. Such behavior is similar to that reported in literatures [21,27,28]. In Fig. 8(b), with an increase in H_{dc}, α_E increases before reaching its maximum of about 33 mV cm^{-1} Oe^{-1} near 1 kOe with H_{ac} = 10 Oe at 1 kHz, and then drops and remains nearly constant beyond 3 kOe. The observed trend is similar to that reported in Ryu et al.'s and Zeng et al.'s work, respectively [29,30]. The bias magnetic field H_{max}, where maximum α_E occurs, is not the coercive field as supposed [31], but close to the field where a maximum magnetostriction and magnetization occur. The α_E vs. H_{dc} curve has a hysteretic nature due to the hysteresis behavior of the constituents. The existence of the remanence is due to the polarization remanence of the PZT component and the charge accumulation on the grain boundaries of the samples [32]. The α_E value is comparable to those obtained in other ME systems such as $CoFe_2O_4$–$BaTiO_3$ ($\alpha_E \approx 3$ mV cm^{-1}Oe^{-1}), $Ni_{0.5}Cu_{0.5}Fe_2O_4/Ba_{0.5}Pb_{0.5}Ti_{0.5}Zr_{0.5}O_3$ ($\alpha_E \approx 0.2$ mV cm^{-1} Oe^{-1}), and $Sr_{1.9}Ca_{0.1}NaNb_5O_{15}$–$CoFe_2O_4$ (SCNN–CFO) ($\alpha_E \approx 58$ mV cm^{-1} Oe^{-1} under a H_{ac} of 10 Oe at

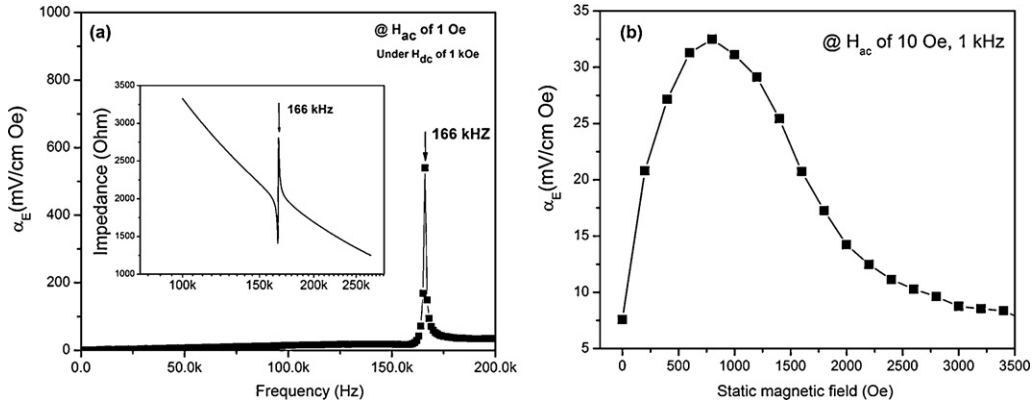

Fig. 8. (a) Frequency dependence of α_E under a condition of H_{dc} = 1 kOe, H_{ac} = 1 Oe and (b) the bias magnetic field (H_{dc}) dependence of α_E under an alternating magnetic field (H_{ac}) at 1 kHz and 10 Oe amplitude. The inset shows data on impedance versus frequency of a poled 15 wt% ceramic.

88 kHz) [14,17,20] at high temperature above 1150 °C. We attribute the high α_E to two possible reasons: (1) high quality of fine-grained microstructures with 3–0 connectivity pattern is obtained in the ceramics fixed at low sintering temperature; (2) an improved interfacial contact and a good mixing of the two individual phases are achieved by a modified hybrid route, thus providing an enhanced ME interaction rate between the two constituent phases. The enhanced ME coupling in the vicinity of electromechanical resonance of the fine-grained ceramics in this work may find promising applications as high-frequency magnetic field sensors, transducers and magnetic field tunable microwave signal processors.

4. Conclusion

Fine-grained PZT–NZFO ME composite ceramics were successfully fabricated by the modified hybrid process at a low sintering temperature of 900 °C. Dense, well-developed, and homogeneous microstructures were obtained with a well-controlled grain size and very good mixing of the two phases in the ceramic body. The composition and purity of the two constituent phases were also maintained after sintering at low temperature. A high ME voltage coefficient (α_E) of 0.537 V cm^{-1} Oe^{-1} was observed in the vicinity of electromechanical resonance with H_{ac} = 1 Oe at 166 kHz and H_{dc} = 1 kOe. At low frequency, the maximum α_E obtained was ~33 mV cm^{-1} Oe− with H_{ac} = 10 Oe at 1 kHz. We attributed the results to the fine-grained microstructure prepared by the modified hybrid process which has a good dispersion and an improved interfacial contact of the two phases. In addition, the magnetic properties of the ceramics can be tailored in a simple and flexible way. On the basis of our studies, it is suggested that fine-grained PZT–NZFO ceramics may be used in a new class of electric circuits and miniature ME devices for high-frequency applications.

Acknowledgements

This work was supported by the Research Grants Council of the HKSAR Government under grant no. PolyU 5266/08E, The Hong Kong Polytechnic University under grant nos. 4-ZZ7T and 1-ZV7P, and NSFC/RGC project no. N_PolyU 501/08.

References

[1] J. Van Suchetelene, Philips Res. Rep. 27 (1972) 28.
[2] N.A. Hill, Annu. Rev. Mater. Res. 32 (2002) 1.
[3] H. Zheng, et al., Science 303 (2004) 661.
[4] M.I. Bichurin, et al., Ferroelectrics 303 (1997) 661.
[5] D.V. Chashin, Y.K. Fetisov, K.E. Kamentsev, G. Srinivasan, Appl. Phys. Lett. 92 (2008) 102511.
[6] Y.J. Wang, S.W. Or, W.H.L. Chan, X.Y. Zhao, H.S. Luo, J. Appl. Phys. 103 (2008) 124511.
[7] Y.J. Wang, S.W. Or, W.H.L. Chan, X.Y. Zhao, H.S. Luo, Appl. Phys. Lett. 92 (2008) 123510.
[8] Y.J. Wang, F.F. Wang, S.W. Or, W.H.L. Chan, X.Y. Zhao, H.S. Luo, Appl. Phys. Lett. 93 (2008) 113503.
[9] C.S. Park, C.W. Ahn, J. Ryu, W.H. Yoon, D.S. Park, H.E. Kim, S. Priya, J. Appl. Phys. 105 (2009) 094111.
[10] N. Cai, J. Zhai, C.W. Nan, Y. Lin, Z. Shi, Phys. Rev. B 68 (2003) 224103.
[11] S.X. Dong, J.Y. Zhai, J.F. Li, D. Viehland, Appl. Phys. Lett. 89 (2006) 243512.
[12] G. Srinivasan, C.P. De Vreugd, Phys. Rev. B 71 (2005) 184423.
[13] G.T. Rado, V.J. Folen, Phys. Rev. Lett. 7 (1961) 310.
[14] C.M. Kanamadi, S.R. Kulkarni, K.K. Patankar, S.S. Chougule, S.J. Patil, B.K. Chougule, J. Mater. Sci. 42 (2007) 5080–5084.
[15] H.F. Zhang, S.W. Or, H.L.W. Chan, J. Appl. Phys. 104 (2008) 104109.
[16] H.F. Zhang, S.W. Or, H.L.W. Chan, Mater. Res. Bull. 44 (2009) 1339–1346.
[17] W.C. Liu, C.L. Mak, K.H. Wong, C.Y. Lo, S.W. Or, W. Zhou, A. Hauser, F.Y. Yang, R. Sooryakumar, J. Phys. D: Appl. Phys. 41 (2008) 125402.
[18] K.K. Patankar, S.A. Patil, K.V. Sivakumar, R.P. Mahajan, Y.D. Kolekar, M.B. Kothale, Mater. Chem. Phys. 65 (2000) 97–102.
[19] S.R. Kulkarni, C.M. Kanamadi, B.K. Chougule, Mater. Res. Bull. 40 (2005) 2064–2072.
[20] G.V. Duong, R. Groessinger, J. Magn. Magn. Mater. 316 (2007) 624–627.
[21] D.A. Filippov, M.I. Bichurin, V.M. Petrov, V.M. Laletin, N.N. Paddubnaya, Proceedings of the 5rd International Conference on Magnetoelectric Interaction Phenomena in Crystals, MEIPIC-5, NATO Advanced Research Workshop at the Touristic Health Complex "Sudak" in Sudak, Ukraine, edited by Manfred Fiebig, Victor V. Eremenko, 2003, pp. 65–70.
[22] Handbook of X-ray Diffraction, 3rd ed., Rigaku, Japan, 1985.
[23] H.F. Zhang, X. YAO, L.Y. ZHANG, J. Am. Ceram. Soc. 90 (2007) 2333–2339.
[24] H.F. Zhang, S.W. Or, W.H.L. Chan, K.W. Kwok, J. Phys. Chem. Solids 70 (2009) 1218–1222.
[25] D.A. Dimitrov, G.M. Wysin, Phys. Rev. B 50 (1994) 3077–3084.
[26] C.G. Koops, Phys. Rev. 83 (1951) 121–124.
[27] V.M. Laletin, V.M. Petrov, D.S. Tuskov, G. Srinivasan, Tech. Phys. Lett. 34 (2008) 83–89.
[28] U. Laletsin, N. Padubnaya, G. Srinivasan, C.P. Devreugd, Appl. Phys. A 78 (2004) 33–36.
[29] J. Ryu, S. Priya, K. Uchino, H.E. Kim, J. Electroceram. 8 (2002) 107–119.
[30] M. Zeng, J.G. Wan, Y. Wang, H. Yu, J.-M. Liu, X.P. Jiang, C.W. Nan, J. Appl. Phys. 95 (2004) 8069–8073.
[31] M. Fiebig, J. Phys. D: Appl. Phys. 38 (2005) 123.
[32] R.S. Singh, T. Bhimasankaram, G.S. Kumar, S.V. Suryanarayana, Solid State Commun. 91 (1994) 567.